

Review

# Research Progress of Tungsten Oxide-Based Catalysts in Photocatalytic Reactions

Zenan Ni \*, Qiuwen Wang, Yuxin Guo \*, Huimin Liu and Qijian Zhang

School of Chemical and Environmental Engineering, Liaoning University of Technology, Jinzhou 121001, China  
\* Correspondence: hgnzn@lnut.edu.cn (Z.N.); gyx313546890@outlook.com (Y.G.)

**Abstract:** Photocatalysis technology is a potential solution to solve the problem of environmental pollution and energy shortage, but its wide application is limited by the low efficiency of solar energy conversion. As a non-toxic and inexpensive n-type semiconductor,  $\text{WO}_3$  can absorb approximately 12% of sunlight which is considered one of the most attractive photocatalytic candidates. However, the narrow light absorption range and the high recombination rate of photogenerated electrons and holes restrict the further development of  $\text{WO}_3$ -based catalysts. Herein, the studies on preparation and modification methods such as doping element, regulating defects and constructing heterojunctions to enlarge the range of excitation light to the visible region and slow down the recombination of carriers on  $\text{WO}_3$ -based catalysts so as to improve their photocatalytic performance are reviewed. The mechanism and application of  $\text{WO}_3$ -based catalysts in the dissociation of water, the degradation of organic pollutants, as well as the hydrogen reduction of  $\text{N}_2$  and  $\text{CO}_2$  are emphatically investigated and discussed. It is clear that  $\text{WO}_3$ -based catalysts will play a positive role in the field of future photocatalysis. This paper could also provide guidance for the rational design of other metallic oxide ( $\text{MO}_x$ ) catalysts for the increasing conversion efficiency of solar energy.

**Keywords:**  $\text{WO}_3$ ; photocatalysis; environment; energy



**Citation:** Ni, Z.; Wang, Q.; Guo, Y.; Liu, H.; Zhang, Q. Research Progress of Tungsten Oxide-Based Catalysts in Photocatalytic Reactions. *Catalysts* **2023**, *13*, 579. <https://doi.org/10.3390/catal13030579>

Academic Editor: Carolina Belver

Received: 21 February 2023

Revised: 6 March 2023

Accepted: 10 March 2023

Published: 13 March 2023



**Copyright:** © 2023 by the authors. Licensee MDPI, Basel, Switzerland. This article is an open access article distributed under the terms and conditions of the Creative Commons Attribution (CC BY) license (<https://creativecommons.org/licenses/by/4.0/>).

## 1. Introduction

With the continuous development of modern society and the continuous growth of the population, global carbon dioxide emissions and industrial wastes are increasing at an alarming rate. Although countries around the world are driving the use of new energy, traditional fossil fuels such as coal, oil and natural gas still play a dominant role in the proportion of energy. Since the use of non-renewable fossil energy will produce carbon dioxide, sulfur dioxide and other gases, researchers are inevitably working to solve the problems of energy shortage, global greenhouse effect, acid rain, PM 2.5 and so on [1–3]. Solar energy is an inexhaustible source of energy. The annual energy of the sun to the earth is  $32 \times 10^{24}$  J, which is 10,000 times the current annual energy consumption of human beings [4]. At the same time, the development and utilization of solar energy will not cause secondary pollution. There is no doubt that solar energy is one of the most promising energy sources, and solar energy is considered to be one of the direct and effective ways to alleviate and solve the current energy crisis and environmental pollution [5].

Metallic oxide ( $\text{MO}_x$ ) semiconductors are important mediums for converting solar energy into chemical energy. When the energy of a photon is equal to or higher than the band gap, electron-hole pairs on the semiconductor could be excited. Then, these carriers would migrate to the surface of the semiconductor and transfer to the adsorbed molecule, eventually starting the reduction or oxidation process [6]. Since the catalytic decomposition of water to produce hydrogen [7] and the dechlorinated polychlorinated biphenyls (organic pollutants) [8] were achieved by semiconductor materials under illumination, photocatalysis technology based on semiconductor materials developed rapidly, showing a good application prospect in solving the problems of energy crisis and environmental

pollution. There are many semiconductor materials in the world. Titanium dioxide (TiO<sub>2</sub>) is undoubtedly one of the most classic photocatalysts, and TiO<sub>2</sub> has attracted wide attention due to its outstanding properties such as chemical stability, non-toxicity, low cost and high light activity [9–11]. The main drawback is that TiO<sub>2</sub> cannot take advantage of visible light, which is due to its large band gap (3.2 eV); the utilization rate of sunlight spectrum is low (only 4%) [12]. As a result, many UV lamps are required to remove the target contaminants during treatment, raising operating costs. The ideal photocatalyst should maximize the use of solar energy. Therefore, WO<sub>3</sub>, which can absorb visible light, has understandably received extensive attention for various photocatalytic reactions.

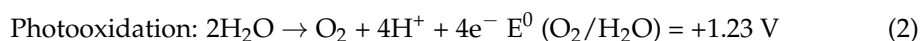
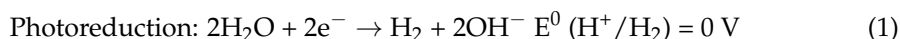
WO<sub>3</sub> is an n-type semiconductor material, whose valence band and conduction band are composed of O 2p orbitals and W 5d orbitals, respectively. WO<sub>3</sub> crystals are composed of multiple WO<sub>6</sub> with regular octahedral structures arranged and combined in the form of common top points [13]. The physical properties of WO<sub>3</sub> are complicated due to structural distortion and oxygen defect. The incline and torsion of crystal structure will cause the change of W 5d energy level leading to the different types of the band gap of WO<sub>3</sub>. In general, monoclinic WO<sub>3</sub> has a band gap of 2.62 eV, while amorphous WO<sub>3</sub> has a band gap of 3.25 eV [14]. Due to the presence of oxygen vacancy in WO<sub>3-x</sub> with non-stoichiometric ratio, the position of O 2d energy level will be changed, thus narrowing the band gap of WO<sub>3-x</sub> to about 1.4–2 eV. The change in band gap will directly affect the light absorption of semiconductor materials and its photocatalytic performance. Usually, the color of WO<sub>3</sub> is light yellow-green, while non-stoichiometric WO<sub>3-x</sub> presents as dark green or bluish-purple with the increase in oxygen defect content. The unique properties of WO<sub>3</sub> make it photochromic and electrochromic equivalents [15].

In recent years, WO<sub>3</sub> has been widely reported in the field of photocatalytic reactions. Most of the existing reviews focus on summarizing the research progress of WO<sub>3</sub>-based catalysts in a specific direction (mostly for the degradation of liquid organic pollutants), but there is a lack of effective discussion on the similarity of synthesis and modification methods of WO<sub>3</sub>-based catalysts, especially for different photocatalytic reactions in the gas and liquid phases. In this paper, the research progress of WO<sub>3</sub>-based catalyst using solar energy to solve the environmental and energy crisis is reviewed, and the common rules and prospects in different synthesis, modification and optimization of WO<sub>3</sub>-based catalyst are provided.

## 2. Application of WO<sub>3</sub>-Based Catalyst

### 2.1. WO<sub>3</sub>-Based Catalyst for Water Splitting

Hydrogen and oxygen have attracted growing interest because they can be used in various fields [16,17]. Photocatalytic water splitting mainly utilize the electrical charges to dissociate water. Typically, photogenerated electrons reduce water molecules to hydrogen, and photogenerated holes oxidize water molecules to oxygen. The specific photocatalytic water splitting reaction is as follows [18]:



The band structure of semiconductors (relative to standard hydrogen electrodes) is summarized in Figure 1 [19]. The water splitting reaction has certain requirements for the band structure of semiconductors. The gap width, valence band position and conduction band position are the prerequisites for the photocatalytic reaction of the semiconductor. In order to initiate the redox reaction, the maximum valence band position of the semiconductor should be more positive than the water oxidation potential (1.23 V). While the lowest conduction position of the semiconductor should be more negative than the water reduction potential (0 V). Therefore, the minimum band gap of the photocatalyst for water splitting reaction is 1.23 eV. On the other hand, holes on the more positive valence band have a higher oxidizing capacity, while electrons on the more negative CB have a stronger

reducing ability [20]. Therefore, this seemingly contradictory relationship must be balanced well according to the specific reaction conditions.

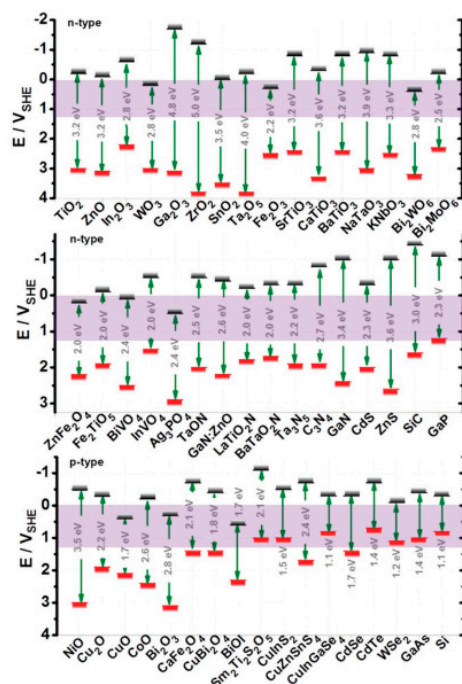


**Figure 1.** Band structure illustration of common semiconductors (vs. normal hydrogen electrode) [19].

### 2.1.1. Water to Oxygen

The photocatalytic properties of  $\text{WO}_3$  with different crystal phases are different [21,22]. Among various crystal phases, the monoclinic phase is the most stable at room temperature and the most widely studied crystal phase. Monocline  $\text{WO}_3$  could absorb visible light ( $E_g = 2.5\text{--}2.8$  eV). The filled O 2p orbital forms the valence band, and the empty W 5d orbital forms the conduction band.  $\text{WO}_3$  has a lower conduction band and the potential is not negative enough to reduce water to hydrogen, but the oxidation potential of the valence band is positive enough to oxidize water to oxygen [20]. So  $\text{WO}_3$  is often used as a catalyst for oxidize water to generate oxygen through under visible light. Here are some representative findings.

Photocatalytic oxygen production performance of  $\text{WO}_3$ /graphene composite photocatalyst synthesized by ultrasonic method [23] is higher than that of  $\text{WO}_3$ , graphene and their simple mixture samples prepared by the same method. By comparing the Raman peak, the researchers found that the chemical bonds between  $\text{WO}_3$ /graphene reduced the interface defects of composite catalyst, thus reducing the recombination probability of photogenerated carriers. In addition, graphene can sensitize  $\text{WO}_3$  so as to expand light absorption range and improve light utilization. Graphene can also be used as a transport medium for photogenerated electrons.

The preparation of pure  $\text{WO}_3$  is also available for photocatalytic reactions. In order to improve the efficiency of solar light harvesting and charge separation, a simple strategy is developed for the synthesis of defect-engineered three-dimensionally ordered macroporous  $\text{WO}_3$  photonic crystals with defect engineering by colloidal crystal template method (Figure 2) [24]. The oxygen evolution rate of the obtained defect-engineered 3DOM  $\text{WO}_3$  (W270–400) is  $40.1 \text{ mmol}\cdot\text{h}^{-1}$ , much higher than fresh 3DOM  $\text{WO}_3$  and defect engineering  $\text{WO}_3$  nanoparticles. The experimental results show that the slow photon effect and the narrow band gap caused by the bulk oxygen vacancy greatly improve the light harvesting efficiency, and the abundant surface oxygen vacancy can reduce the valence band as well as increase the power of water oxidation, thus significantly promoting the separation of electrons and holes.

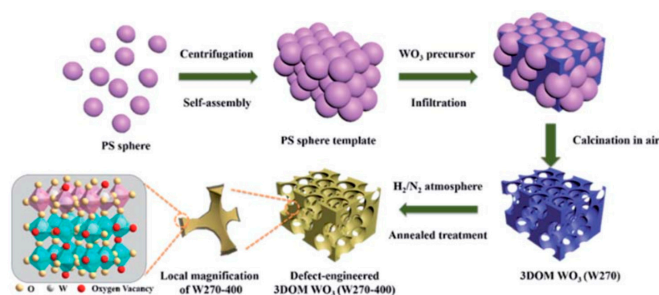


**Figure 2.** Schematic illustration of the preparation of 3DOM  $\text{WO}_3$  [24].

The  $\text{Ag}_3\text{PO}_4/\text{WO}_3$  S-scheme heterojunction synthesized via deposition-precipitation process showed better photocatalytic activity in oxygen production ( $306.6 \mu\text{mol}\cdot\text{L}^{-1}\cdot\text{h}^{-1}$ ) than pure  $\text{Ag}_3\text{PO}_4$  ( $204.4 \mu\text{mol}\cdot\text{L}^{-1}\cdot\text{h}^{-1}$ ) under visible light (Figure 3) [25]. It shows that  $\text{Ag}_3\text{PO}_4/\text{WO}_3$  with a suitable ratio endowed the heterojunction with strong redox abilities to drive the photocatalytic reaction.

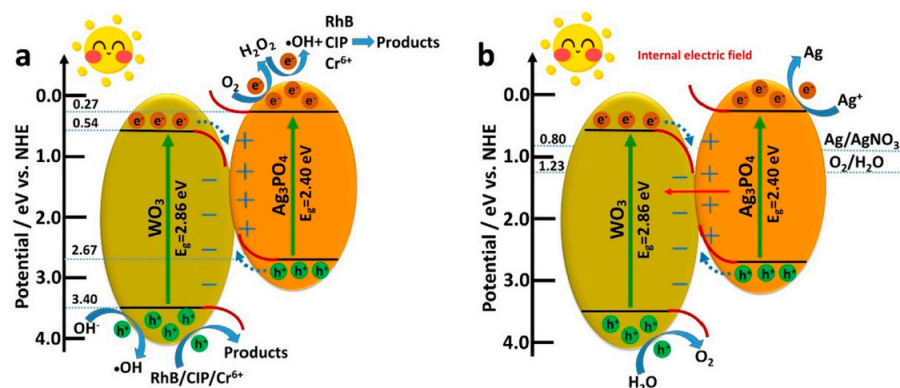


**Figure 3.** Schematic illustration of  $\text{Ag}_3\text{PO}_4/\text{WO}_3$  S-scheme mechanism for photocatalytic degradation and  $\text{O}_2$  evolution [25]. (a) oxidizing RhB/CIP/ $\text{Cr}^{6+}$  to  $\text{CO}_2$  and  $\text{H}_2\text{O}$ , (b) water splitting to generate  $\text{O}_2$ .

Though assembling porous  $\text{WO}_3$  shells on the outer surface of hollow carbon nitride spheres (HCNS), three-dimensional (3D) Z-scheme  $\text{WO}_3@\text{HCNS}$  hollow nano hybrids with intimate interfacial contacts were constructed [26], and the catalyst was evaluated by water oxidation to generate oxygen under visible light ( $\lambda > 420 \text{ nm}$ ). The high oxygen evolution rate of ( $23 \mu\text{mol}\cdot\text{h}^{-1}$ ) over  $\text{WO}_3@\text{HCNS}$  is about 20 times that of the original HCNS ( $1.2 \mu\text{mol}\cdot\text{h}^{-1}$ ). The excellent performance of  $\text{WO}_3@\text{HCNS}$  is mainly due to its Z-scheme hollow heterostructures with strong coupling interface, which promotes the separation and migration of charge carriers, and facilitates the shuttle of mass transport. This work may inspire the future production of nano HCN Z-scheme heterostructures with custom shells and tight connections that serve as efficient platforms for photocatalytic  $\text{H}_2\text{O}$  splitting.

### 2.1.2. Water to Hydrogen

The physical and chemical properties of  $\text{WO}_3$  material are rich and adjustable. Reasonable combination with other components could also be used to convert water to hydrogen via  $\text{WO}_3$ -based catalysts.

Photocatalytic water splitting is an uphill reaction, and the recombination of photoexcited electrons and holes is very serious. Methanol as an electron donor or silver ion as an electron acceptor is often used in photocatalytic hydrogen-producing and oxygen-producing reactions. These substances are more reactive than water and would be consumed in the reaction, known as sacrificial agents. For example, the standard hydrogen electrode potential for

reduction of formic acid to methanol is  $E(\text{HCOOH}/\text{CH}_3\text{OH}) = +0.04 \text{ V}$ , while the standard hydrogen electrode potential for oxygen reduction to water is  $E(\text{O}_2/\text{H}_2\text{O}) = +1.23 \text{ V}$  [27].

It was reported that  $\text{g-C}_3\text{N}_4/\text{WO}_3$ -carbon microsphere-based photocatalysts are prepared by the one-pot thermal method for converting water into hydrogen [28]. The efficiency of hydrogen production is 107.75 times and 70.54 times greater than that of pure  $\text{g-C}_3\text{N}_4$  under visible light and sunlight irradiation, respectively. This is because that the carbon microspheres make the catalyst have good conductivity and promote the transfer of photogenerated electrons in  $\text{g-C}_3\text{N}_4$  nanosheets.

$\text{WO}_3/\text{g-C}_3\text{N}_4$  with extended nanojunctions was prepared via the novel sol-gel method which can control zeta potential and sol-gel phase [29]. The composite catalyst exhibited improved UV-vis absorbance and reduced the recombination rate of photogenerated electron-hole pairs.

Zinc porphyrin-assembled nanorods (ZnTPyP) and  $\text{WO}_3$  nanorods' nanorod-on-nanorod heterojunctions ( $\text{ZnTPyP}/\text{WO}_3$ ) exhibited a great hydrogen production rate ( $74.53 \text{ mmol}\cdot\text{g}^{-1}\cdot\text{h}^{-1}$ ) due to the direct Z-scheme electron-transfer mechanism from  $\text{WO}_3$  to ZnTPyP (Figure 4) [30]. The direct Z-scheme can effectively improve the separation efficiency of photogenerated carriers.

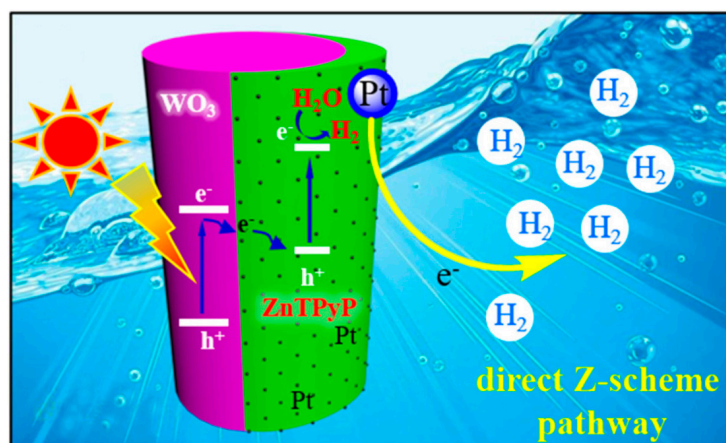


**Figure 4.** Photocatalytic mechanism scheme and the possible charge separation of direct Z-scheme  $\text{ZnTPyP}/\text{WO}_3$  [30].

$\text{CdS}/\text{WO}_3$  composites prepared by the self-assemble method were used to study the charge transfer direction in  $\text{CdS}/\text{WO}_3$  heterojunction and photocatalytic mechanism [31]. The  $\text{CdS}/\text{WO}_3$  composites with mass ratio ( $\text{CdS}:\text{WO}_3$ ) of 1:3 have the best hydrogen production efficiency. The electrons and holes migration mechanism used in the  $\text{CdS}/\text{WO}_3$  heterojunction was the Z-scheme, which kept the redox capability of the catalyst while facilitating the separation of photogenerated carriers.

Defects also play a key role in the activity of photocatalysts. Broadband transient absorption spectroscopy was used to study the effects of oxygen vacancies on photocarrier dynamics in  $\text{WO}_3$  [32]. This work provides us an important conclusion. When the defect is dispersed, the trapped electrons need to travel long distances between defects by jumping and tunneling repeatedly to bind to the hole, resulting in deceleration recombination. On the contrary, when defects join or come close together, trapped electrons can easily migrate between defects, resulting in faster recombination.

According to the discussion in Section 2.1, it can be clearly concluded that  $\text{WO}_3$ -based catalysts can be used in photocatalytic water splitting to produce both hydrogen and oxygen by the addition of other components, and creating sufficient difficulty for the recombination of electrons and holes via heterojunction; defects and sacrificial reagents form the research direction of  $\text{WO}_3$ -based catalysts.

## 2.2. WO<sub>3</sub>-Based Catalyst for Degradation

### 2.2.1. Liquid Organic Pollutant

In modern society, the surge of the global population and human demand for textiles have made the pollution problem in the process of textiles prominent. In particular, the discharge of textile dye wastewater has become a difficult problem to solve regarding the pollution of textile dye [33]. Textile dyes are difficult to degrade naturally, so the green technology of semiconductor is needed to solve this problem. Good visible light absorption and electron conduction ability provide WO<sub>3</sub> with great advantages in the photodegradation of organic pollutants [34–37]. However, due to the high recombination rate of photogenerated carrier, the photodegradation performance in the application of pure WO<sub>3</sub> is not good enough. The catalytic activity of WO<sub>3</sub> can be improved by combining with other semiconductors [38] or doping other metal [39] or non-metal ions [40]. Representatively, liquid organic pollutants mainly discussed in this section include methylene blue (MB), methylene orange (MO), and rhodamine B (RhB). Some representative research results are as follows.

For example, WO<sub>3</sub>/Ag<sub>3</sub>PO<sub>4</sub> composite catalyst [41] prepared by hydrothermal synthesis method was used to decompose MB and MO pollutants under visible light. Compared with pure Ag<sub>3</sub>PO<sub>4</sub> and pure WO<sub>3</sub>, WO<sub>3</sub>/Ag<sub>3</sub>PO<sub>4</sub> showed excellent catalytic performance. Therewith, many composite catalysts with better catalytic performance based on WO<sub>3</sub> and Ag<sub>3</sub>PO<sub>4</sub> have been reported. Sea urchin WO<sub>3-x</sub> was successfully prepared by hydrothermal method and then gradually deposited Ag<sub>3</sub>PO<sub>4</sub> [42]. In this work, Ag<sup>+</sup> was reduced into Ag by W<sup>5+</sup> and Ag deposited on the surface of WO<sub>3-x</sub> with sea urchin structure. This structure can effectively reduce the recombination rate of photogenerated electrons and holes. The degradation performance of Ag<sub>3</sub>PO<sub>4</sub>/Ag/WO<sub>3-x</sub> catalyst was four times higher than that of pure Ag<sub>3</sub>PO<sub>4</sub>. Furthermore, a type Z-heterogeneous Ag/Ag<sub>3</sub>PO<sub>4</sub>/WO<sub>3</sub> catalyst was prepared by depositional precipitation and photoreduction method [43]. By adjusting the pH value, it was observed that Ag/Ag<sub>3</sub>PO<sub>4</sub>/WO<sub>3</sub> showed higher degradation efficiency for RhB under neutral or even strong acid and alkali environment. WO<sub>3</sub>(H<sub>2</sub>O)<sub>0.333</sub>/Ag<sub>3</sub>PO<sub>4</sub> composite was prepared by stirring method and microwave hydrothermal method (Figure 5) [44], proving that the prepared Z-type catalytic mechanism composite can also broaden the range of response to visible light. After five cycles, the degradation efficiency of 15% WO<sub>3</sub>(H<sub>2</sub>O)<sub>0.333</sub>/Ag<sub>3</sub>PO<sub>4</sub> was still higher than that of pure Ag<sub>3</sub>PO<sub>4</sub>.

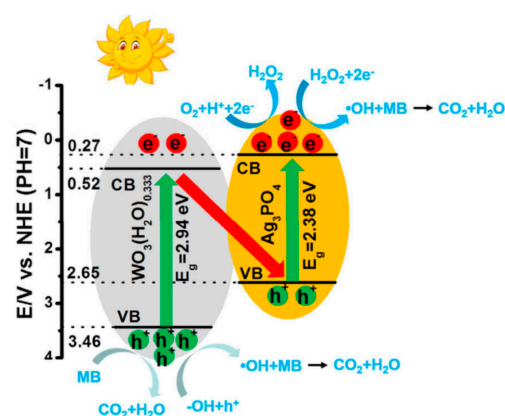


**Figure 5.** The photocatalytic mechanism of WO<sub>3</sub>(H<sub>2</sub>O)<sub>0.333</sub>/Ag<sub>3</sub>PO<sub>4</sub> composites under visible light [44].

WO<sub>3</sub> with hollow spherical photocatalyst with different layers synthesized using carbon spheres as the template, and the sample showed excellent photodegradation effect on RhB [45]. A network WO<sub>3</sub>·0.33H<sub>2</sub>O was prepared by adding inorganic salts. After 7 h of simulated solar irradiation, this sample could remove about 95% of MB [46]. The WO<sub>3</sub>/graphene composite photocatalyst could remove about 92% MO under xenon lamp irradiation for 120 min [47].

In addition to the discussion above, there are also other good results about the use of metal or nonmetal doped  $\text{WO}_3$  in the degradation of liquid pollutants that have been reported. Improving the photo response range of  $\text{WO}_3$ -based catalysts is one of the main research directions. Some representative research results are shown in Table 1.

**Table 1.** Application of doped  $\text{WO}_3$  for photocatalytic removal of contaminants.

| Catalyst           | Method                            | $E_{bg}$ (eV) | Radiation Source | Contaminant  | Removal (Time)                      | Ref. |
|--------------------|-----------------------------------|---------------|------------------|--|-------------------------------------|------|
| Ag- $\text{WO}_3$  | Hydrothermal, HCl                 | 2.63          | Solar            | Acetaminophen, 5 mg L <sup>-1</sup>  | 75.4% (120 min)                     | [48] |
| Cd- $\text{WO}_3$  | Ion-exchange                      | 1.85          | Visible          | Methylene Blue, 10 mg L <sup>-1</sup>  | 75.5% (80 min)                      | [49] |
| Co- $\text{WO}_3$  | Co-precipitation                  | -             | Visible          | Methyl Red, 10 mg L <sup>-1</sup>  | 90% (120 min)                       | [50] |
| Cu- $\text{WO}_3$  | Precipitation                     | 2.6           | Visible          | Tetracycline, 50 mg L <sup>-1</sup>  | 96.7% (120 min)                     | [51] |
| Fe- $\text{WO}_3$  | Sol-gel                           | 2.39          | Visible          | Methylene Blue, 10 mg L <sup>-1</sup>  | 95% (120 min)                       | [52] |
| Gd- $\text{WO}_3$  | Hydrothermal                      | 2.64          | Visible          | Rhodamine B, 20 mg L <sup>-1</sup>   | 94% (100 min)                       | [53] |
| Ni- $\text{WO}_3$  | Co-precipitation                  | 2.25          | Visible          | Methyl Red, 20 mg L <sup>-1</sup>  | 96% (120 min)                       | [54] |
| Mn- $\text{WO}_3$  | Microwave-assisted, Precipitation | 2             | Visible          | Sulfamethoxazole, 1 mg L <sup>-1</sup>   | 100% (70 min)                       | [55] |
| C- $\text{WO}_3$   | Hydrothermal                      | -             | UV-Visible       | Rhodamine B, 20 mg L <sup>-1</sup>   | 95% (180 min)                       | [56] |
| I- $\text{WO}_3$   |                                   | 2.17          |                  |  | 88.2% TOC<br>89.1% COD<br>(240 min) |      |
| P- $\text{WO}_3$   | Hydrolysis and Precipitation      | 2.41          | Solar            | Dyeing Wastewater, Total organic carbon =576.8 mg L <sup>-1</sup> , chemical, and biological oxygen demand =991 mg L <sup>-1</sup> | 86.8% TOC<br>86.6% COD<br>(240 min) | [57] |
| P-I- $\text{WO}_3$ |                                   | 2.02          |                  |  | 93.4% TOC<br>95.1% COD<br>(240 min) |      |
| S- $\text{WO}_3$   | Hydrothermal                      | -             | Visible          | Methyl orange, 20 mg L <sup>-1</sup>   | 97% (180 min)                       | [58] |
|                    | Hydrothermal                      | 2.46          | Visible          | Methylene Blue, 10 mg L <sup>-1</sup>  | 79% (120 min)                       | [59] |

## 2.2.2. Vapor Organic Pollutant

Organic pollutants that  $\text{WO}_3$  can degrade are not limited to liquid pollutants, but also indoor vapor pollutants. With the increasing demand for comfortable working and living spaces, furniture and decorative materials are widely used in rooms, houses and buildings [60]. However, these materials contain large amounts of adhesives such as formaldehyde (HCHO) and phenolic resins, which can cause serious indoor air pollution. The removal of indoor HCHO is of practical significance [61,62]. At present, physical adsorption, biodegradation, catalytic oxidation and other methods have obtained better removal effects of HCHO. Among them, catalytic oxidation could completely convert HCHO into harmless carbon dioxide ( $\text{CO}_2$ ), which shows the maximum efficiency [63,64].

HCHO absorption behavior towards the  $\text{WO}_{2.9}(010)$  surface was studied using the first principles calculations for the first time [65]. Its total energy calculation results indicated that the excellent absorption properties for HCHO molecules on  $\text{WO}_{2.9}(010)$ , and a substoichiometric  $\text{WO}_{2.9}(010)$  surface is appropriate for HCHO sensing and elimination at room temperature under visible light irradiation.

The layered-WO<sub>3</sub> catalyst with hollow microspheres was prepared by solution method and then loaded with Pt (Figure 6) [66]. It was reported that the optimal deposition amount of Pt was determined to be 1.0 wt%, and the layered hollow structure endowed more active sites for diffusion and transfer of Pt/WO<sub>3</sub>. DRFITS spectral analysis results showed that the main intermediates were formate and dioxymethylene species, which were further decomposed into CO<sub>2</sub> and H<sub>2</sub>O.

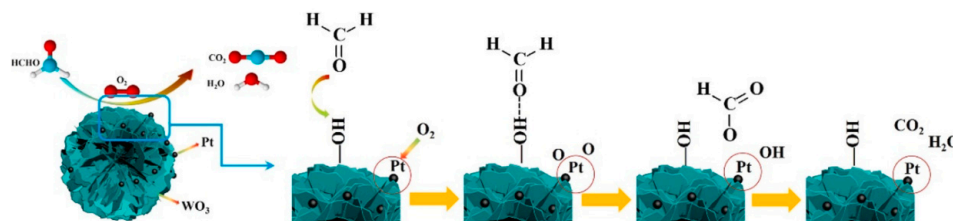


**Figure 6.** Possible mechanism of HCHO decomposition on the Pt/WO<sub>3</sub> catalysts [66].

Nano-structure Fe-doped WO<sub>3</sub>-modified solid wood was prepared interestingly, and HCHO was self-photodegraded under visible light (Figure 7) [67]. The spherical Fe-doped WO<sub>3</sub> nanomaterials deposited on wood substrate have strong adhesion to wood surface through electrostatic and hydrogen bonding interactions. In total, 98.21% of HCHO was effectively degraded within 6 h. Nanostructured WO<sub>3</sub> materials significantly improve and eliminate wood dimensional stability and inherent anisotropic thickness expansion, respectively.

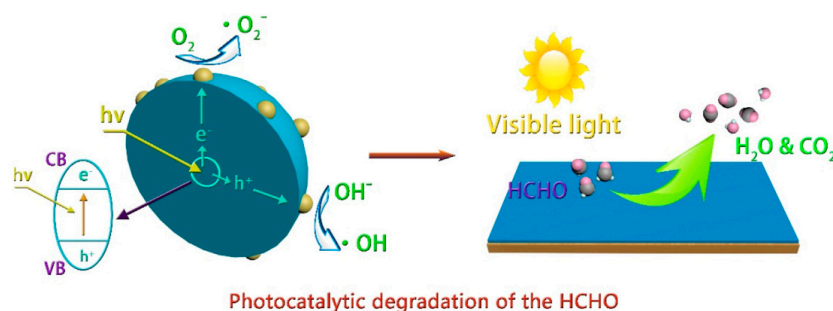


**Figure 7.** Schematic illustration of photocatalytic degradation of HCHO to CO<sub>2</sub> and H<sub>2</sub>O by wood covered with Fe-doped WO<sub>3</sub> [67].

Different contaminant degradation reactions put forward higher requirements for the preparation of WO<sub>3</sub> catalyst, and the structure of multi-component (metal/WO<sub>3</sub> and MO<sub>x</sub>/WO<sub>3</sub>) catalyst must be more specific in terms of the active site. In addition, reaction conditions (pH and illumination) gradually become important.

### 2.3. WO<sub>3</sub>-Based Catalyst for CO<sub>2</sub> Reduction

The excessive use of fossil fuels has caused a significant increase in the emission of CO<sub>2</sub> greenhouse gases, which has seriously damaged the carbon cycle balance in nature [68–70]. However, CO<sub>2</sub> itself is a carbon resource, which can be used as a raw material for the preparation of carbon-based compounds. The conversion of CO<sub>2</sub> into high-value fuels helps to alleviate energy shortage and environmental crisis at the same time. Bio-catalysis, thermochemical conversion, electrocatalysis and photocatalysis can convert CO<sub>2</sub> into carbon-based compounds [71–75], among which photocatalytic reduction can directly utilize clean and sustainable solar energy to convert CO<sub>2</sub> into carbon-based fuel at room temperature and atmospheric pressure, which is regarded as a CO<sub>2</sub> conversion method with more application prospects.

However, the actual conversion efficiency of the CO<sub>2</sub> photocatalytic reduction is relatively low [76,77], due to insufficient utilization of sunlight and limited photoelectron reduction ability. Early CO<sub>2</sub> reduction photocatalysts can only use ultraviolet light (UV,  $\lambda < 400$  nm) [78,79]. In order to improve the utilization rate of sunlight and improve the

performance of CO<sub>2</sub> reduction and conversion, a variety of visible light catalysts have been designed and synthesized, such as g-C<sub>3</sub>N<sub>4</sub>, BiOBr, CdS, etc. [80–82]. However, the infrared light, which accounts for nearly 50% of the sunlight, has not been fully utilized. It is known that the UV-visible region mainly induces photocatalytic reaction, while the infrared region is the main heat producing region (IR,  $\lambda > 800$  nm), whose energy can drive both photocatalytic and thermo-catalytic reactions. As reported in the literature, infrared photo-responsive materials mainly include noble metal nanoparticles (such as Au, Ag, Pt) [83,84], carbon nanomaterials (such as graphene, carbon nanotubes, polypyrrole) [85], narrow band gap semiconductor materials (such as Bi<sub>2</sub>S<sub>3</sub>, MXene, black phosphorus) [86,87] and a few heavily-doped MO<sub>x</sub> (such as MoO<sub>3-x</sub>, W<sub>18</sub>O<sub>40</sub>) [88,89].

The catalytic efficiency of CO<sub>2</sub> photoreduction is determined by light absorption, charge separation and surface reaction rate (Figure 8) [90]. Loading nano-cocatalyst on the surface of semiconductor catalyst can enhance the photo-charge separation efficiency, and then regulate the photocatalytic conversion performance of CO<sub>2</sub> [75,91]. The reported relevant studies mostly focus on noble metal cocatalysts, which usually improve CO<sub>2</sub> reduction efficiency through electron transfer [91]. However, in the photocatalytic conversion of CO<sub>2</sub> with H<sub>2</sub>O as proton source, the migration of photogenerated holes is equally important [92,93]. MO<sub>x</sub> clusters were often used as electron or hole cocatalysts due to their composition [94]. There was usually a strong interaction between oxygen vacancy and MO<sub>x</sub> clusters loading on the surface, which was conducive to the high dispersion of catalyst on the WO<sub>3-x</sub> surface [95].

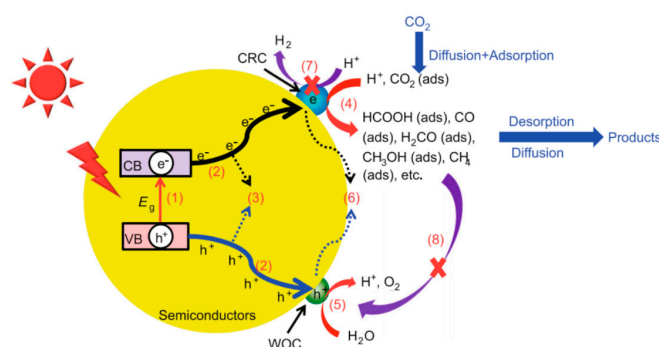


**Figure 8.** Processes involved in photocatalytic CO<sub>2</sub> reduction over a heterogeneous photocatalyst. CRC, CO<sub>2</sub> reduction co-catalysts; WOC, water oxidation co-catalysts [90].

In terms of experimental conditions, CO<sub>2</sub> reduction is an endothermic reaction, therefore, introducing heat into the photocatalytic system may have a better effect. In the views of catalyst design, the introduction of oxygen vacancy can regulate the electronic structure of WO<sub>3-x</sub> and form a new intermediate energy level in its band structure, thus generating near-infrared light response and local temperature rise on the catalyst surface. In addition, the introduction of cocatalyst can regulate the WO<sub>3-x</sub> conduction potential and enhance the separation and migration of photogenerated charge by trapping light holes.

#### 2.4. WO<sub>3</sub>-Based Catalyst for N<sub>2</sub> Reduction

Artificial synthesis of ammonia (NH<sub>3</sub>) by reducing atmospheric N<sub>2</sub> is of great importance to human society [96]. The industrial Haber-Bosch process of producing NH<sub>3</sub> from N<sub>2</sub> and H<sub>2</sub> is usually performed on Fe-based catalysts under harsh conditions (300–450 °C, 15–25 MPa), with significant energy consumption and fossil-derived CO<sub>2</sub> emissions [97]. Therefore, an energy-saving and environmentally-friendly NH<sub>3</sub> synthesis method is needed. Using a semiconductor for N<sub>2</sub> reduction at room temperature and atmospheric pressure is a promising strategy [98], and photocatalysis for N<sub>2</sub> fixation provides an interesting method. It also relies on light-excited electrons being transferred to a stable N≡N bond. Bottlenecks occur when N<sub>2</sub> is chemically adsorbed at active sites (surface defects) and N<sub>2</sub>

molecules cannot be effectively activated and dissociated by high energy electrons. Many experiments have been carried out and some important results are listed below.

Since Schrauzer and Guth's pioneering work on photocatalytic  $N_2$  fixation on  $TiO_2$ -based catalysts [99–101], solar-powered  $N_2$  fixation has been considered a promising alternative to the traditional Haber-Bosch process. However, the wide band gap, the poor interaction between catalyst and  $N_2$  molecule, and the high energy of  $N_2$  intermediate make it difficult for  $TiO_2$ -based semiconductor photocatalysis to fix  $N_2$  [102,103]. Notably,  $WO_3$  semiconductors are considered to have good water oxidation properties due to their appropriate band structure [104]. Efficient  $N_2$  photo-fixation of  $NH_3$  is achieved by the carbon- $WO_3 \cdot H_2O$  hybrid in pure water without any additives or auxiliary catalysts [105]. It was found that carbon greatly promotes the activation of  $N_2$  at the surface and the separation as well as transport of photogenerated carriers. Moreover, photoactive  $WO_3 \cdot H_2O$  had excellent electron/proton conductivity, ensuring the supply of electrons and protons required for subsequent protonation.

A full-spectrum-absorption heterojunction catalyst  $W_{18}O_{49}/g-C_3N_4$  was prepared and used for the first time to simulate  $N_2$  photo-fixation under solar irradiation (Figure 9) [106]. The research shows found that  $g-C_3N_4$  was the real active component of heterojunction reduction catalyst, while  $W_{18}O_{49}$  acted as an absorbent in the full spectrum, forming more photogenerated electrons and reorganizing the holes in  $g-C_3N_4$  via the “Z-scheme” mechanism.  $W_{18}O_{49}(0.6)/g-C_3N_4$  showed the highest  $r(NH_4^{+})$  at  $2.6 \text{ mg} \cdot \text{L}^{-1} \cdot \text{h}^{-1} \cdot \text{g}_{\text{cat}}^{-1}$ , 7.2-times higher than pure  $g-C_3N_4$ . This was due to the improved separation rate of electron-hole pairs after coupling with  $W_{18}O_{49}$ .

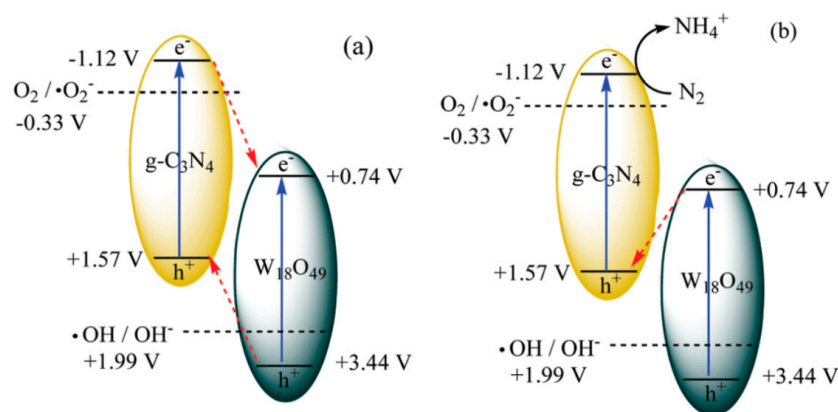


**Figure 9.** The possible double charge transfer mechanism (a) and the Z-scheme mechanism (b) over  $W_{18}O_{49}(0.6)/g-C_3N_4$  [106].

$g-C_3N_4/Cs_xWO_3$  composites could also effectively reduce  $N_2$  from the atmosphere to  $NH_3$  under full spectrum light, without the need for any noble metal auxiliary catalyst [107]. Oxygen may also play an active role in the conversion of  $N_2$  to ammonia synthesis, when the methanol content is properly controlled.

The bottleneck of  $N_2$  activation and deionization can be well resolved by doping to refine the defect state of the semiconductor [108]. Considering the critical role of defects as catalytic active sites, this refinement can regulate both chemisorption and electron transfer of  $N_2$ . The doping of Mo promotes the efficient movement of photoexcited electrons towards  $N_2$ , impelling  $N \equiv N$  bond dissociation and  $N_2$  reduction.

In the photocatalytic reduction of  $N_2$ , the regulation of heterojunction, morphology, and defects are considered as effective modification strategies. As a method to change the electronic structure and chemical properties of semiconductors to affect the adsorption and activation behavior of  $N_2$ , defect engineering exhibits a broader prospect. By introducing appropriate defects, the separation and migration of carrier would be boosted. Then, light absorption efficiency could be improved, surface redox reaction could be enhanced and the catalytic reaction path may be adjusted to a certain extent.

### 3. Design and Preparation of WO<sub>3</sub>-Based Catalyst

The common preparation methods of WO<sub>3</sub>-based catalyst are mainly based on the hydrothermal method, the colloidal crystal template method and the deposition-precipitation method. For different photocatalytic reactions, the preparation methods of catalysts are flexible and abundant, but the rational design of the whole catalyst is the premise of choosing the preparation method. Photocatalytic reaction is a complex physicochemical process, and the charge dynamics involved mainly include the generation, separation, migration, recombination and surface capture of photogenerated electrons and holes [5,109]. Based on this information, the design and preparation of WO<sub>3</sub>-based catalyst should start from the analysis of the main factors affecting each charge dynamic process in the photocatalytic reaction process, and improve the overall efficiency of the photocatalytic reaction process by expanding the wavelength range of light absorption, improving the separation and transfer efficiency of electron hole pairs, and changing the selectivity and yield of products.

#### 3.1. The Efficiency of Light Absorption

The band structure of a semiconductor determines its ability to absorb light, therefore, the band structure of the semiconductor needs to be adjusted to absorb a wider range of wavelengths. The band structure of semiconductor is not only determined by its own crystal phase and vacancy, but also modified by doping negative and cation in the crystal or surface of the semiconductor. By adjusting these factors, the band gap of semiconductor can be narrowed, the absorption range of sunlight wavelength can be expanded, and the activity of catalyst can be improved.

#### 3.2. Separation and Migration of Electron and Hole

When the semiconductor photocatalyst is photoexcited, the electron hole pairs generated inside will separate and migrate to the surface of the catalyst, and directly react with the adsorbed substances on the surface. The earlier electrons and holes migrate to the reaction site, the less likely they are to recombine. So, regulating the separation efficiency and diffusion path of electron hole pairs is the key to improve the photocatalytic reaction efficiency [110]. In addition, defects inside or on the surface of the semiconductor can also become composite centers of photogenerated electrons and holes, which can also lead to limitations in the efficiency of charge transfer. In semiconductor composite structures, the effective charge transfer between semiconductors also depends on electronic coupling at their interfaces, so the internal electric field and potential difference driving forces can improve the separation and migration efficiency of photogenerated electron hole pairs [111].

#### 3.3. Surface Reaction

The photocatalytic reaction occurs only on the surface of the catalyst in both the gas phase and liquid phase systems. In this process, the reactants first diffuse and adsorb to the surface of the catalyst, and then undergo reduction reactions and oxidation reactions with electrons and holes that migrate to the surface. The resulting reduction products and oxidation products will cause desorption from the surface and diffuse into the environment after the reaction. Therefore, the process of adsorption-desorption and molecular activation essentially determines the catalytic activity of the surface reaction, and increasing the adsorption energy of the catalyst surface or decreasing the activation energy of the catalyst surface can enhance the catalytic reaction kinetic process. In the photocatalytic system, surface factors such as the specific surface area and pores of the material, the exposure of active crystal surface, surface composition and surface vacancy will affect the activity and selectivity of the catalyst [112]. Increasing the specific surface area and pores of the catalyst enables more reactants to contact the surface atoms, thus increasing the possibility of interaction between the catalytic active site and the reactant. The exposure ratio of the active crystal surface of the catalyst is closely related to the separation and transfer efficiency of photogenerated electron-hole pairs, atomic arrangement on the material

surface, activation energy and other factors [113]. Of course, not all surface atoms can effectively participate in photocatalytic reactions. Photogenerated carriers and reactants tend to migrate more readily to vacancies on the catalyst surface. Hence, increasing the density of the surface vacancy can enhance the adsorption and activation process of the catalyst to the target molecules, thus improving the surface reaction efficiency.

#### 4. Challenges and Perspectives

Issues surrounding energy and the environment are absolutely inescapable for everyone. Solar energy-chemical energy conversion technology is very important to solve the environmental problems and energy crisis, and studying the use of solar energy will provide a great contribution to the sustainable development of the social economy.  $\text{WO}_3$  has attracted much attention because of its stable physical and chemical properties, low cost and simple preparation process. Based on the research of  $\text{WO}_3$  in different photocatalytic directions by researchers around the world in recent years, this paper summarized the existing problems of  $\text{WO}_3$  as a photocatalyst in the current research stage, the corresponding solutions and the essential reasons for better photocatalytic performance in different photocatalytic reactions. There are various modification and optimization methods for  $\text{WO}_3$ -based catalysts, including doping other elements, tailoring the type, population as well as distribution of defects, and constructing-regulating the heterojunction. Increasing the density of the semiconductor carrier, expanding the absorption of sunlight and balancing the relationship among valence band, conduction band and band width, the object of all research methods above aims to improve the photocatalytic effect of  $\text{WO}_3$ -based catalysts for dissociation of water, degradation of organic pollutants, as well as the reduction of  $\text{CO}_2$  and  $\text{N}_2$ .

Researchers have put a lot of effort into the development of different  $\text{WO}_3$  photocatalysts and have advanced the field in many directions. It is worth noting that there is still a long way for  $\text{WO}_3$ -based catalysts from being developed and designed to benefit humans on a larger scale. Here are some of the challenges  $\text{WO}_3$ -based catalysts faces and what future science experiments could focus on. (1). The current photocatalytic conditions are too ideal compared with natural light, because the stability of sunlight irradiation includes the interference of humidity, impurities and other factors along the propagation path. Therefore, improving the photocatalytic stability of catalysts directly under sunlight will advance the development of photocatalysis. (2). Due to the high recombination rate of electron and hole of  $\text{WO}_3$ , the quantum efficiency of photocatalytic reaction is low and its application is limited. The development of efficient  $\text{WO}_3$ -based photocatalyst through the design and controllable synthesis of material is a key problem that must be solved to promote the practical application of  $\text{WO}_3$  photocatalytic technology. (3). Many noble metals and sacrificial agents are used for water splitting, which increases the cost of in the dissociation of water, the degradation of organic pollutants, as well as the hydrogen reduction of  $\text{N}_2$  and  $\text{CO}_2$ . Therefore, cheaper catalysts should be developed as soon as possible. (4). For the analysis of different reaction mechanism of photocatalyst, it is necessary to use spherical correction electron microscopy, in situ infrared spectroscopy, transient absorption spectroscopy, scanning electrochemical microscopy and other advanced detection technologies to analyze the state of doping atoms in the lattice, the lifetime of photogenerated carrier and intermediate state species in the process of photocatalytic reaction, so as to further study and reveal the mechanism of photocatalytic reaction.

#### 5. Conclusions

$\text{WO}_3$  is a well-known semiconductor photocatalyst due to its good response in the solar spectrum, fine metal interactions, mechanical strength, high efficiency, harmlessness and cost-effectiveness. Based on the analysis and summary, it can be clearly found that the commonality of regulatory strategies of  $\text{WO}_3$ -based catalysts is to expose more active sites and keep its strong redox capacity, thus benefiting the improvement of photocatalytic performance. Although  $\text{WO}_3$  materials have been extensively studied in the field of

photocatalysis, the mechanism of photocatalysis has not been systematically studied. For example, the transport mechanism of photogenerated charge in different heterojunction is not clear, and the analysis of deep and micro-scale photocatalysis mechanism is still a big challenge. The combination of experiment and calculation may be a good starting point. Therefore, exploring the mechanism of enhanced  $\text{WO}_3$  photocatalytic activity and establishing relationship between the structure of catalyst and the performance of main reaction are significant to promote the research process of photocatalytic materials.

Another point worth noting is the combined use of multiple energy sources. Because the catalysis based on single energy source is likely to suffer from technical bottlenecks, therefore, sufficient attention should be paid to the collaboration of photovoltaic energy or photoelectric energy, and even the collaboration of photothermal and photoelectronic energy, as long as it serves the sustainable development of human beings and alleviates environmental problems and energy crisis. For example, when the irradiation conditions are unstable on cloudy days, it may be surprising when the introduction of the suitable amount of heat energy can supplement the power for the conversion of reactant.

**Author Contributions:** Conceptualization, Z.N.; methodology, Z.N. and Y.G.; software, Z.N.; validation, Q.W., H.L. and Q.Z.; formal analysis, H.L.; investigation, Z.N. and Y.G.; resources, Z.N., Y.G. and Q.Z.; data curation, Z.N. and Y.G.; writing—original draft preparation, Z.N.; writing—review and editing, H.L. and Q.Z.; funding acquisition, Z.N., Y.G. and Q.Z. All authors have read and agreed to the published version of the manuscript.

**Funding:** This research is funded by Foundation of Liaoning Province Education Department of China, grant number LJKMZ20220982 and Foundation of Liaoning Province Education Department of China, grant number LJKQZ20222297; Liaoning Province Applied Basic Research program, grant number 2022JH2/101300125.

**Data Availability Statement:** Not applicable.

**Conflicts of Interest:** The authors declare sincerely that they have no known competing financial interest or personal relationship that could have appeared to influence the work reported in this paper.

## References

1. Maggard, P.A. Capturing metastable oxide semiconductors for applications in solar energy conversion. *Acc. Chem. Res.* **2021**, *54*, 3160–3171. [[CrossRef](#)]
2. Li, J.; Zeng, H.; Dong, X.; Ding, Y.; Hu, S.; Zhang, R.; Dai, Y.; Cui, P.; Xiao, Z.; Zhao, D.; et al. Selective  $\text{CO}_2$  electrolysis to CO using isolated antimony alloyed copper. *Nat. Commun.* **2023**, *14*, 340–350. [[CrossRef](#)]
3. Hepburn, C.; Adlen, E.; Beddington, J.; Carter, E.A.; Fuss, S.; Mac Dowell, N.; Minx, J.C.; Smith, P.; Williams, C.K. The technological and economic prospects for  $\text{CO}_2$  utilization and removal. *Nature* **2019**, *575*, 87–97. [[CrossRef](#)]
4. Grätzel, M. Powering the planet. *Nature* **2000**, *403*, 363–364. [[CrossRef](#)]
5. Li, X.; Yu, J.; Jaroniec, M. Hierarchical photocatalysts. *Chem. Soc. Rev.* **2016**, *45*, 2603–2636. [[CrossRef](#)]
6. Mateo, D.; Cerrillo, J.L.; Durini, S.; Gascon, J. Fundamentals and applications of photo-thermal catalysis. *Chem. Soc. Rev.* **2021**, *50*, 2173–2210. [[CrossRef](#)]
7. Fujishima, A.; Honda, K. Electrochemical photolysis of water at a semiconductor electrode. *Nature* **1972**, *238*, 37–38. [[CrossRef](#)]
8. Carey, J.H.; Lawrence, J.; Tosine, H.M. Photodechlorination of PCB's in the presence of titanium dioxide in aqueous suspensions. *Bull. Environ. Contam. Toxicol.* **1976**, *16*, 697–701. [[CrossRef](#)] [[PubMed](#)]
9. Chen, X.; Mao, S.S. Titanium dioxide nanomaterials synthesis, properties, modifications, and applications. *Chem. Rev.* **2007**, *107*, 2891–2959. [[CrossRef](#)]
10. Liu, C.; Wang, L.; Tang, Y.; Luo, S.; Liu, Y.; Zhang, S.; Zeng, Y.; Xu, Y. Vertical single or few-layer  $\text{MoS}_2$  nanosheets rooting into  $\text{TiO}_2$  nanofibers for highly efficient photocatalytic hydrogen evolution. *Appl. Catal. B Environ.* **2015**, *164*, 1–9. [[CrossRef](#)]
11. Yang, X.; Dai, W.; Guo, C.; Chen, H.; Cao, Y.; Li, H.; He, H.; Fan, K. Synthesis of novel core-shell structured  $\text{WO}_3/\text{TiO}_2$  spheroids and its application in the catalytic oxidation of cyclopentene to glutaraldehyde by aqueous  $\text{H}_2\text{O}_2$ . *J. Catal.* **2005**, *234*, 438–450. [[CrossRef](#)]
12. He, X.; Wang, A.; Wu, P.; Tang, S.; Zhang, Y.; Li, L.; Ding, P. Photocatalytic degradation of microcystin-LR by modified  $\text{TiO}_2$  photocatalysis: A review. *Sci. Total Environ.* **2020**, *743*, 140694. [[CrossRef](#)] [[PubMed](#)]
13. Roussel, P.; Labbe, P.; Groult, D. Symmetry and twins in the monophosphate tungsten bronze series  $(\text{PO}_2)_4(\text{WO}_3)_{2m}$  ( $2 \leq m \leq 14$ ). *Acta Crystallogr.* **2000**, *56*, 377–391. [[CrossRef](#)]
14. Gillet, M.; Aguir, K.; Lemire, C.; Gillet, E.; Schierbaum, K. The structure and electrical conductivity of vacuum-annealed  $\text{WO}_3$  thin films. *Thin Solid Film.* **2004**, *467*, 239–246. [[CrossRef](#)]

15. Nah, Y.-C.; Ghicov, A.; Kim, D.; Schmuki, P. Enhanced electrochromic properties of self-organized nanoporous WO<sub>3</sub>. *Electrochem. Commun.* **2008**, *10*, 1777–1780. [[CrossRef](#)]
16. Luo, S.; Lin, H.; Wang, Q.; Ren, X.; Hernandez-Pinilla, D.; Nagao, T.; Xie, Y.; Yang, G.; Li, S.; Song, H.; et al. Triggering water and methanol activation for solar-driven H<sub>2</sub> production: Interplay of dual active sites over plasmonic zinc alloy. *J. Am. Chem. Soc.* **2021**, *143*, 12145–12153. [[CrossRef](#)] [[PubMed](#)]
17. Sharaf, O.Z.; Orhan, M.F. An overview of fuel cell technology: Fundamentals and applications. *Renew. Sustain. Energy Rev.* **2014**, *32*, 810–853. [[CrossRef](#)]
18. Jafari, T.; Moharreri, E.; Amin, A.S.; Miao, R.; Song, W.; Suib, S.L. Photocatalytic water splitting—the untamed dream: A review of recent advances. *Molecules* **2016**, *21*, 900. [[CrossRef](#)]
19. Xiao, M.; Wang, Z.; Lyu, M.; Luo, B.; Wang, S.; Liu, G.; Cheng, H.M.; Wang, L. Hollow nanostructures for photocatalysis: Advantages and challenges. *Adv. Mater.* **2019**, *31*, 900–923. [[CrossRef](#)]
20. Wang, Y.; Tian, W.; Chen, C.; Xu, W.; Li, L. Tungsten trioxide nanostructures for photoelectrochemical water splitting: Material engineering and charge carrier dynamic manipulation. *Adv. Funct. Mater.* **2019**, *29*, 1809036–1809050. [[CrossRef](#)]
21. Dong, P.; Hou, G.; Xi, X.; Shao, R.; Dong, F. WO<sub>3</sub>-based photocatalysts: Morphology control, activity enhancement and multifunctional applications. *Environ. Sci. Nano* **2017**, *4*, 539–557. [[CrossRef](#)]
22. Samuel, O.; Othman, M.H.D.; Kamaludin, R.; Sinsamphanh, O.; Abdullah, H.; Puteh, M.H.; Kurniawan, T.A. WO<sub>3</sub>-based photocatalysts: A review on synthesis, performance enhancement and photocatalytic memory for environmental applications. *Ceram. Int.* **2022**, *48*, 5845–5875. [[CrossRef](#)]
23. Guo, J.; Li, Y.; Zhu, S.; Chen, Z.; Liu, Q.; Zhang, D.; Moon, W.-J.; Song, D.-M. Synthesis of WO<sub>3</sub>@Graphene composite for enhanced photocatalytic oxygen evolution from water. *RSC Adv.* **2012**, *2*, 1356–1363. [[CrossRef](#)]
24. Wang, Y.; Peng, C.; Jiang, T.; Zhang, J.; Jiang, Z.; Li, X. Construction of defect-engineered three-dimensionally ordered macroporous WO<sub>3</sub> for efficient photocatalytic water oxidation reaction. *J. Mater. Chem. A* **2021**, *9*, 3036–3043. [[CrossRef](#)]
25. Li, D.; Liu, Y.; Yang, Y.; Tang, G.; Tang, H. Rational construction of Ag<sub>3</sub>PO<sub>4</sub>/WO<sub>3</sub> step-scheme heterojunction for enhanced solar-driven photocatalytic performance of O<sub>2</sub> evolution and pollutant degradation. *J. Colloid Interface Sci.* **2022**, *608*, 2549–2559. [[CrossRef](#)]
26. Zheng, D.; Chen, W.; Huang, Z.; Wang, S. Coating hollow carbon nitride nanospheres with porous WO<sub>3</sub> shells to construct Z-scheme heterostructures for efficient photocatalytic water oxidation. *ChemPhotoChem* **2022**, *6*, e202200143. [[CrossRef](#)]
27. Maeda, K.; Domen, K. Photocatalytic water splitting: Recent progress and future challenges. *J. Phys. Chem. Lett.* **2010**, *1*, 2655–2661. [[CrossRef](#)]
28. Sun, M.; Zhou, Y.; Yu, T.; Wang, J. Synthesis of g-C<sub>3</sub>N<sub>4</sub>/WO<sub>3</sub>-carbon microsphere composites for photocatalytic hydrogen production. *Int. J. Hydrogen Energy* **2022**, *47*, 10261–10276. [[CrossRef](#)]
29. Won, J.H.; Kim, M.K.; Oh, H.-S.; Jeong, H.M. Scalable production of visible light photocatalysts with extended nanojunctions of WO<sub>3</sub>/g-C<sub>3</sub>N<sub>4</sub> using zeta potential and phase control in sol-gel process. *Appl. Surf. Sci.* **2023**, *612*, 155838. [[CrossRef](#)]
30. Liu, S.; Xia, S.; Wang, J.; Ren, X.; Chen, S.; Zhong, Y.; Bai, F. Synthesis of the ZnTPyP/WO<sub>3</sub> nanorod-on-nanorod heterojunction direct Z-scheme with spatial charge separation ability for enhanced photocatalytic hydrogen generation. *Nanoscale* **2023**, *15*, 2871–2881. [[CrossRef](#)] [[PubMed](#)]
31. Xiong, X.; Jin, Y.; Wang, H.; He, P.; Xiang, X.; Hu, P.; Liu, K.; Wei, Q.; Wang, B. Study on the hydrogen production properties and electron transfer mechanism of CdS/WO<sub>3</sub> composite photocatalyst. *Mater. Chem. Phys.* **2022**, *281*, 125824–125831. [[CrossRef](#)]
32. Kato, K.; Uemura, Y.; Asakura, K.; Yamakata, A. Role of oxygen vacancy in the photocarrier dynamics of WO<sub>3</sub> photocatalysts: The case of recombination centers. *J. Phys. Chem. C* **2022**, *126*, 9257–9263. [[CrossRef](#)]
33. Sonu, K.; Sogani, M.; Syed, Z.; Dongre, A.; Sharma, G. Enhanced decolorization and treatment of textile dye wastewater through adsorption on acid modified corncob derived biochar. *ChemistrySelect* **2020**, *5*, 12287–12297. [[CrossRef](#)]
34. VafaeiAsl, M.; Keshavarz, I.; Shemirani, F.; Jamshidi, P. Green synthesis of a novel magnetic Fe<sub>3</sub>O<sub>4</sub>@SiO<sub>2</sub>/TiO<sub>2</sub>@WO<sub>3</sub> nanocomposite for methylene blue removal under UV and visible light irradiations. *Res. Chem. Intermed.* **2023**, *23*, 1–15. [[CrossRef](#)]
35. Bhardwaj, R.; Thakur, U.N.; Ajmera, P.; Singhal, R.; Rosenwaks, Y.; Hazra, A. Field-assisted sensitivity amplification in a noble metal nanoparticle decorated WO<sub>3</sub>/GO hybrid fet-based multisensory array for selective detection of breath acetone. *ChemNanoMat* **2022**, *8*, e202100448. [[CrossRef](#)]
36. Stan, M.; Toloman, D.; Popa, A.; Dan, M.; Suci, R.C.; Macavei, S.; Tripon, S.C.; Chaiseeda, K.; Pana, O. Facile synthesis of MWCNT-WO<sub>3</sub> composites with enhanced photocatalytic degradation of methylene blue dye. *Synth. Met.* **2022**, *288*, 117117. [[CrossRef](#)]
37. Tahir, M.B.; Nabi, G.; Rafique, M.; Khalid, N.R. Nanostructured-based WO<sub>3</sub> photocatalysts: Recent development, activity enhancement, perspectives and applications for wastewater treatment. *Int. J. Environ. Sci. Technol.* **2017**, *14*, 2519–2542. [[CrossRef](#)]
38. Faris, A.H.; Hamid, K.J.; Naji, A.M.; Mohammed, M.K.A.; Nief, O.A.; Jabir, M.S. Novel Mo-doped WO<sub>3</sub>/ZnO nanocomposites loaded with polyvinyl alcohol towards efficient visible-light-driven photodegradation of methyl orange. *Mater. Lett.* **2023**, *334*, 133746–133750. [[CrossRef](#)]
39. Yang, H.; Zhao, Z.-C.; Yang, Y.-P.; Zhang, Z.; Chen, W.; Yan, R.-Q.; Jin, Y.; Zhang, J. Defective WO<sub>3</sub> nanoplates controllably decorated with MIL-101(Fe) nanoparticles to efficiently remove tetracycline hydrochloride by S-scheme mechanism. *Sep. Purif. Technol.* **2022**, *300*, 121846–121856. [[CrossRef](#)]

40. Seifollahi Bazarjani, M.; Hojamberdiev, M.; Morita, K.; Zhu, G.; Cherkashinin, G.; Fasel, C.; Herrmann, T.; Breitzke, H.; Gurlo, A.; Riedel, R. Visible light photocatalysis with c-WO<sub>3-x</sub>/WO<sub>3</sub>×H<sub>2</sub>O nanoheterostructures in situ formed in mesoporous polycarbosilane-siloxane polymer. *J. Am. Chem. Soc.* **2013**, *135*, 4467–4475. [[CrossRef](#)] [[PubMed](#)]
41. Lu, J.; Wang, Y.; Liu, F.; Zhang, L.; Chai, S. Fabrication of a direct Z-scheme type WO<sub>3</sub>/Ag<sub>3</sub>PO<sub>4</sub> composite photocatalyst with enhanced visible-light photocatalytic performances. *Appl. Surf. Sci.* **2017**, *393*, 180–190. [[CrossRef](#)]
42. Bu, Y.; Chen, Z.; Sun, C. Highly efficient Z-Scheme Ag<sub>3</sub>PO<sub>4</sub>/Ag/WO<sub>3-x</sub> photocatalyst for its enhanced photocatalytic performance. *Appl. Catal. B Environ.* **2015**, *179*, 363–371. [[CrossRef](#)]
43. Li, Q.; Wang, F.; Hua, Y.; Luo, Y.; Liu, X.; Duan, G.; Yang, X. Deposition-precipitation preparation of Ag/Ag<sub>3</sub>PO<sub>4</sub>/WO<sub>3</sub> nanocomposites for efficient Visible-light degradation of rhodamine B under strongly acidic/alkaline conditions. *J. Colloid Interface Sci.* **2017**, *506*, 207–216. [[CrossRef](#)] [[PubMed](#)]
44. Li, Z.; Wang, X.; Zhang, J.; Liang, C.; Lu, L.; Dai, K. Preparation of Z-scheme WO<sub>3</sub>(H<sub>2</sub>O)<sub>0.333</sub>/Ag<sub>3</sub>PO<sub>4</sub> composites with enhanced photocatalytic activity and durability. *Chin. J. Catal.* **2019**, *40*, 326–334. [[CrossRef](#)]
45. Xi, G.; Yan, Y.; Ma, Q.; Li, J.; Yang, H.; Lu, X.; Wang, C. Synthesis of multiple-shell WO<sub>3</sub> hollow spheres by a binary carbonaceous template route and their applications in visible-light photocatalysis. *Chem.–A Eur. J.* **2012**, *18*, 13949–13954. [[CrossRef](#)]
46. He, X.; Hu, C.; Yi, Q.; Wang, X.; Hua, H.; Li, X. Preparation and improved photocatalytic activity of WO<sub>3</sub>·0.33H<sub>2</sub>O nanonetworks. *Catal. Lett.* **2012**, *142*, 637–645. [[CrossRef](#)]
47. Zhou, M.; Yan, J.; Cui, P. Synthesis and enhanced photocatalytic performance of WO<sub>3</sub> nanorods @ graphene nanocomposites. *Mater. Lett.* **2012**, *89*, 258–261. [[CrossRef](#)]
48. Hasse Palharim, P.; Lara Diego dos Reis Fusari, B.; Ramos, B.; Otubo, L.; Silva Costa Teixeira, A.C. Effect of HCl and HNO<sub>3</sub> on the synthesis of pure and silver-based WO<sub>3</sub> for improved photocatalytic activity under sunlight. *J. Photochem. Photobiol. A Chem.* **2022**, *422*, 113550–113561. [[CrossRef](#)]
49. Abu Hanif, M.; Akter, J.; Akherul Islam, M.; Sapkota, K.P.; Hahn, J.R. Visible-light-driven enhanced photocatalytic performance using cadmium-doping of tungsten (VI) oxide and nanocomposite formation with graphitic carbon nitride disks. *Appl. Surf. Sci.* **2021**, *565*, 150541–150553. [[CrossRef](#)]
50. Mehmood, F.; Iqbal, J.; Jan, T.; Gul, A.; Mansoor, Q.; Faryal, R. Structural, photoluminescence, electrical, anti cancer and visible light driven photocatalytic characteristics of Co doped WO<sub>3</sub> nanoplates. *Vib. Spectrosc.* **2017**, *93*, 78–89. [[CrossRef](#)]
51. Quyen, V.T.; Kim, J.; Park, P.-M.; Huong, P.T.; Viet, N.M.; Thang, P.Q. Enhanced the visible light photocatalytic decomposition of antibiotic pollutant in wastewater by using Cu doped WO<sub>3</sub>. *J. Environ. Chem. Eng.* **2021**, *9*, 104737–104743. [[CrossRef](#)]
52. Luxmi, V.; Kumar, A. Enhanced photocatalytic performance of m-WO<sub>3</sub> and m-Fe-doped WO<sub>3</sub> cuboids synthesized via sol-gel approach using egg albumen as a solvent. *Mater. Sci. Semicond. Process.* **2019**, *104*, 104690–104700. [[CrossRef](#)]
53. Govindaraj, T.; Mahendran, C.; Marnadu, R.; Shkir, M.; Manikandan, V.S. The remarkably enhanced visible-light-photocatalytic activity of hydrothermally synthesized WO<sub>3</sub> nanorods: An effect of Gd doping. *Ceram. Int.* **2021**, *47*, 4267–4278. [[CrossRef](#)]
54. Mehmood, F.; Iqbal, J.; Ismail, M.; Mehmood, A. Ni doped WO<sub>3</sub> nanoplates: An excellent photocatalyst and novel nanomaterial for enhanced anticancer activities. *J. Alloys Compd.* **2018**, *746*, 729–738. [[CrossRef](#)]
55. Yazdanbakhsh, A.; Eslami, A.; Massoudinejad, M.; Avazpour, M. Enhanced degradation of sulfamethoxazole antibiotic from aqueous solution using Mn-WO<sub>3</sub>/LED photocatalytic process: Kinetic, mechanism, degradation pathway and toxicity reduction. *Chem. Eng. J.* **2020**, *380*, 122497–122511. [[CrossRef](#)]
56. Zheng, Y.; Chen, G.; Yu, Y.; Zhou, Y.; He, F. Synthesis of carbon doped WO<sub>3</sub>·0.33H<sub>2</sub>O hierarchical photocatalyst with improved photocatalytic activity. *Appl. Surf. Sci.* **2016**, *362*, 182–190. [[CrossRef](#)]
57. Tijani, J.O.; Ugochukwu, O.; Fadipe, L.A.; Bankole, M.T.; Abdulkareem, A.S.; Roos, W.D. Photocatalytic degradation of local dyeing wastewater by iodine-phosphorus co-doped tungsten trioxide nanocomposites under natural sunlight irradiation. *J. Environ. Manag.* **2019**, *236*, 519–533. [[CrossRef](#)]
58. Han, F.; Li, H.; Fu, L.; Yang, J.; Liu, Z. Synthesis of S-doped WO<sub>3</sub> nanowires with enhanced photocatalytic performance towards dye degradation. *Chem. Phys. Lett.* **2016**, *651*, 183–187. [[CrossRef](#)]
59. Chen, G.; Wang, Q.; Zhao, Z.; Gao, L.; Li, X. Synthesis and photocatalytic activity study of S-doped WO<sub>3</sub> under visible light irradiation. *Environ. Sci. Pollut. Res. Int.* **2020**, *27*, 15103–15112. [[CrossRef](#)]
60. Xie, J.; Wang, S.; Zhao, K.; Wu, M.; Wang, F. Regulating the Pt-MnO<sub>2</sub> interaction and interface for room temperature formaldehyde oxidation. *Inorg. Chem.* **2023**, *62*, 904–915. [[CrossRef](#)]
61. Miao, L.; Wang, J.; Zhang, P. Review on manganese dioxide for catalytic oxidation of airborne formaldehyde. *Appl. Surf. Sci.* **2019**, *466*, 441–453. [[CrossRef](#)]
62. Wang, F.; Wang, Y.; Han, K.; Yu, H. Efficient elimination of formaldehyde over Pt/Fe<sub>3</sub>O<sub>4</sub> catalyst at room temperature. *J. Environ. Chem. Eng.* **2020**, *8*, 104041–104048. [[CrossRef](#)]
63. Wang, S.; Wang, Y.; Wang, F. Room temperature HCHO oxidation over the Pt/CeO<sub>2</sub> catalysts with different oxygen mobilities by changing ceria shapes. *Appl. Catal. A Gen.* **2022**, *630*, 118469–118477. [[CrossRef](#)]
64. Zheng, J.Y.; Zhou, K.L.; Zhao, W.K.; Wang, Y.; He, J.; Wang, X.; Wang, H.; Yan, H.; Han, C.B. Enhanced the synergistic degradation effect between active hydroxyl and reactive oxygen species for indoor formaldehyde based on platinum atoms modified MnOOH/MnO<sub>2</sub> catalyst. *J. Colloid Interface Sci.* **2022**, *628*, 359–370. [[CrossRef](#)]
65. Wang, D.; Han, D.; Liu, L.; Niu, L. Sub-stoichiometric WO<sub>2.9</sub> for formaldehyde sensing and treatment: A first-principles study. *J. Mater. Chem. A* **2016**, *4*, 14416–14422. [[CrossRef](#)]

66. Le, Y.; Qi, L.; Wang, C.; Song, S. Hierarchical Pt/WO<sub>3</sub> nanoflakes assembled hollow microspheres for room-temperature formaldehyde oxidation activity. *Appl. Surf. Sci.* **2020**, *512*, 145763–145770. [[CrossRef](#)]
67. Sheng, C.; Wang, C.; Wang, H.; Jin, C.; Sun, Q.; Li, S. Self-photodegradation of formaldehyde under visible-light by solid wood modified via nanostructured Fe-doped WO<sub>3</sub> accompanied with superior dimensional stability. *J. Hazard. Mater.* **2017**, *328*, 127–139. [[CrossRef](#)] [[PubMed](#)]
68. Roth, F.; Broman, E.; Sun, X.; Bonaglia, S.; Nascimento, F.; Prytherch, J.; Bruchert, V.; Lundevall Zara, M.; Brunberg, M.; Geibel, M.C.; et al. Methane emissions offset atmospheric carbon dioxide uptake in coastal macroalgae, mixed vegetation and sediment ecosystems. *Nat. Commun.* **2023**, *14*, 42–52. [[CrossRef](#)]
69. Han, Y.; Cao, L.; Geng, Z.; Ping, W.; Zuo, X.; Fan, J.; Wan, J.; Lu, G. Novel economy and carbon emissions prediction model of different countries or regions in the world for energy optimization using improved residual neural network. *Sci. Total Environ.* **2023**, *860*, 160410–160422. [[CrossRef](#)]
70. Macedo, P.; Madaleno, M. Global temperature and carbon dioxide nexus: Evidence from a maximum entropy approach. *Energies* **2022**, *16*, 277. [[CrossRef](#)]
71. Sharifzadeh, M.; Wang, L.; Shah, N. Integrated biorefineries: CO<sub>2</sub> utilization for maximum biomass conversion. *Renew. Sustain. Energy Rev.* **2015**, *47*, 151–161. [[CrossRef](#)]
72. Jia, J.; Qian, C.; Dong, Y.; Li, Y.F.; Wang, H.; Ghossoub, M.; Butler, K.T.; Walsh, A.; Ozin, G.A. Heterogeneous catalytic hydrogenation of CO<sub>2</sub> by metal oxides: Defect engineering-perfecting imperfection. *Chem. Soc. Rev.* **2017**, *46*, 4631–4644. [[CrossRef](#)] [[PubMed](#)]
73. Shen, H.; Gu, Z.; Zheng, G. Pushing the activity of CO<sub>2</sub> electroreduction by system engineering. *Sci. Bull.* **2019**, *64*, 1805–1816. [[CrossRef](#)] [[PubMed](#)]
74. Inoue, T.; Fujishima, A.; Konishi, S.; Honda, K. Photoelectrocatalytic reduction of carbon dioxide in aqueous suspensions of semiconductor powders. *Nature* **1979**, *277*, 637–638. [[CrossRef](#)]
75. Li, X.; Yu, J.; Jaroniec, M.; Chen, X. Cocatalysts for selective photoreduction of CO<sub>2</sub> into solar fuels. *Chem. Rev.* **2019**, *119*, 3962–4179. [[CrossRef](#)]
76. Ji, Y.; Luo, Y. Theoretical study on the mechanism of photoreduction of CO<sub>2</sub> to CH<sub>4</sub> on the anatase TiO<sub>2</sub>(101) surface. *ACS Catal.* **2016**, *6*, 2018–2025. [[CrossRef](#)]
77. Zhao, L.; Ye, F.; Wang, D.; Cai, X.; Meng, C.; Xie, H.; Zhang, J.; Bai, S. Lattice engineering on metal cocatalysts for enhanced photocatalytic reduction of CO<sub>2</sub> into CH<sub>4</sub>. *ChemSusChem* **2018**, *11*, 3524–3533. [[CrossRef](#)]
78. Liu, L.; Zhao, H.; Andino, J.M.; Li, Y. Photocatalytic CO<sub>2</sub> reduction with H<sub>2</sub>O on TiO<sub>2</sub> nanocrystals: Comparison of anatase, rutile, and brookite polymorphs and exploration of surface chemistry. *ACS Catal.* **2012**, *2*, 1817–1828. [[CrossRef](#)]
79. Li, P.; Hu, H.; Luo, G.; Zhu, S.; Guo, L.; Qu, P.; Shen, Q.; He, T. Crystal facet-dependent CO<sub>2</sub> photoreduction over porous ZnO nanocatalysts. *ACS Appl. Mater. Interfaces* **2020**, *12*, 56039–56048. [[CrossRef](#)] [[PubMed](#)]
80. Wang, S.; Zhan, J.; Chen, K.; Ali, A.; Zeng, L.; Zhao, H.; Hu, W.; Zhu, L.; Xu, X. Potassium-doped g-C<sub>3</sub>N<sub>4</sub> achieving efficient visible-light-driven CO<sub>2</sub> reduction. *ACS Sustain. Chem. Eng.* **2020**, *8*, 8214–8222. [[CrossRef](#)]
81. Cho, K.M.; Kim, K.H.; Park, K.; Kim, C.; Kim, S.; Al-Saggaf, A.; Gereige, I.; Jung, H.-T. Amine-functionalized graphene/CdS composite for photocatalytic reduction of CO<sub>2</sub>. *ACS Catal.* **2017**, *7*, 7064–7069. [[CrossRef](#)]
82. Zhang, Z.; Li, L.; Jiang, Y.; Xu, J. Step-scheme photocatalyst of CsPbBr<sub>3</sub> quantum dots/BiOBr nanosheets for efficient CO<sub>2</sub> photoreduction. *Inorg. Chem.* **2022**, *61*, 3351–3360. [[CrossRef](#)]
83. Cai, X.; Zhu, M.; Elbanna, O.A.; Fujitsuka, M.; Kim, S.; Mao, L.; Zhang, J.; Majima, T. Au nanorod photosensitized La<sub>2</sub>Ti<sub>2</sub>O<sub>7</sub> nanosteps: Successive surface heterojunctions boosting visible to near-infrared photocatalytic H<sub>2</sub> evolution. *ACS Catal.* **2017**, *8*, 122–131. [[CrossRef](#)]
84. Liu, S.; Chai, J.; Sun, S.; Zhang, L.; Yang, J.; Fu, X.; Hai, J.; Jing, Y.H.; Wang, B. Site-selective photosynthesis of Ag-AgCl@Au nanomushrooms for NIR-II light-driven O<sub>2</sub>- and O<sub>2</sub>-evolving synergistic photothermal therapy against deep hypoxic tumors. *ACS Appl. Mater. Inter.* **2021**, *13*, 46451–46463. [[CrossRef](#)]
85. Moon, H.K.; Lee, S.H.; Choi, H.C. In vivo near-infrared mediated tumor destruction by photothermal effect of carbon nanotubes. *ACS Nano* **2009**, *3*, 3707–3713. [[CrossRef](#)]
86. Chen, X.; Li, Q.; Li, J.; Chen, J.; Jia, H. Modulating charge separation via in situ hydrothermal assembly of low content Bi<sub>2</sub>S<sub>3</sub> into UiO-66 for efficient photothermocatalytic CO<sub>2</sub> reduction. *Appl. Catal. B Environ.* **2020**, *270*, 118915–118925. [[CrossRef](#)]
87. Li, R.; Zhang, L.; Shi, L.; Wang, P. MXene Ti<sub>3</sub>C<sub>2</sub>: An effective 2D light-to-heat conversion material. *ACS Nano* **2017**, *11*, 3752–3759. [[CrossRef](#)] [[PubMed](#)]
88. Kuwahara, Y.; Yoshimura, Y.; Haematsu, K.; Yamashita, H. Mild deoxygenation of sulfoxides over plasmonic molybdenum oxide hybrid with dramatic activity enhancement under visible light. *J. Am. Chem. Soc.* **2018**, *140*, 9203–9210. [[CrossRef](#)] [[PubMed](#)]
89. Li, J.; Ye, Y.; Ye, L.; Su, F.; Ma, Z.; Huang, J.; Xie, H.; Doronkin, D.E.; Zimina, A.; Grunwaldt, J.-D.; et al. Sunlight induced photo-thermal synergistic catalytic CO<sub>2</sub> conversion via localized surface plasmon resonance of MoO<sub>3-x</sub>. *J. Mater. Chem. A* **2019**, *7*, 2821–2830. [[CrossRef](#)]
90. Li, X.; Wen, J.; Low, J.; Fang, Y.; Yu, J. Design and fabrication of semiconductor photocatalyst for photocatalytic reduction of CO<sub>2</sub> to solar fuel. *Sci. China Mater.* **2014**, *57*, 70–100. [[CrossRef](#)]

91. Wang, S.; Teramura, K.; Hisatomi, T.; Domen, K.; Asakura, H.; Hosokawa, S.; Tanaka, T. Highly selective photocatalytic conversion of carbon dioxide by water over Al-SrTiO<sub>3</sub> photocatalyst modified with silver–metal dual cocatalysts. *ACS Sustain. Chem. Eng.* **2021**, *9*, 9327–9335. [[CrossRef](#)]
92. Wang, Y.; Godin, R.; Durrant, J.R.; Tang, J. Efficient hole trapping in carbon dot/oxygen-modified carbon nitride heterojunction photocatalysts for enhanced methanol production from CO<sub>2</sub> under neutral conditions. *Angew. Chem. Int. Ed.* **2021**, *60*, 20811–20816. [[CrossRef](#)]
93. Wang, Y.; Chen, E.; Tang, J. Insight on reaction pathways of photocatalytic CO<sub>2</sub> conversion. *ACS Catal.* **2022**, *12*, 7300–7316. [[CrossRef](#)]
94. Yin, G.; Nishikawa, M.; Nosaka, Y.; Srinivasan, N.; Atarashi, D.; Sakai, E.; Miyauchi, M. Photocatalytic carbon dioxide reduction by copper oxide nanocluster-grafted niobate nanosheets. *ACS Nano* **2015**, *9*, 2111–2119. [[CrossRef](#)] [[PubMed](#)]
95. Billo, T.; Fu, F.Y.; Raghunath, P.; Shown, I.; Chen, W.F.; Lien, H.T.; Shen, T.H.; Lee, J.F.; Chan, T.S.; Huang, K.Y.; et al. Ni-nanocluster modified black TiO<sub>2</sub> with dual active sites for selective photocatalytic CO<sub>2</sub> reduction. *Small* **2018**, *14*, 1702928–1702938. [[CrossRef](#)] [[PubMed](#)]
96. Giddey, S.; Badwal, S.P.S.; Kulkarni, A. Review of electrochemical ammonia production technologies and materials. *Int. J. Hydrogen Energy* **2013**, *38*, 14576–14594. [[CrossRef](#)]
97. Bluhm, M.E.; Bradley, M.G.; Butterick, R.; Kusari, U.; Sneddon, L.G. Amineborane-based chemical hydrogen storage: Enhanced ammonia borane dehydrogenation in ionic liquids. *J. Am. Chem. Soc.* **2006**, *128*, 7748–7749. [[CrossRef](#)]
98. Rusina, O.; Eremenko, A.; Frank, G.; Strunk, H.P.; Kisch, H. Photofixierung von Stickstoff an nanostrukturierten Eisentitanatfilmen. *Angew. Chem. Int. Ed.* **2001**, *113*, 4115–4117. [[CrossRef](#)]
99. Schrauzer, G.N.; Guth, T.D. Photolysis of water and photoreduction of nitrogen on titanium dioxide. *J. Am. Chem. Soc.* **1977**, *99*, 7189–7193. [[CrossRef](#)]
100. Medford, A.J.; Hatzell, M.C. Photon-driven nitrogen fixation: Current progress, thermodynamic considerations, and future outlook. *ACS Catal.* **2017**, *7*, 2624–2643. [[CrossRef](#)]
101. Zhao, Y.; Zhao, Y.; Waterhouse, G.I.N.; Zheng, L.; Cao, X.; Teng, F.; Wu, L.Z.; Tung, C.H.; O'Hare, D.; Zhang, T. Layered-double-hydroxide nanosheets as efficient visible-light-driven photocatalysts for dinitrogen fixation. *Adv. Mater.* **2017**, *29*, 1703828–1703837. [[CrossRef](#)]
102. Liang, Y.T.; Vijayan, B.K.; Gray, K.A.; Hersam, M.C. Minimizing graphene defects enhances titania nanocomposite-based photocatalytic reduction of CO<sub>2</sub> for improved solar fuel production. *Nano Lett.* **2011**, *11*, 2865–2870. [[CrossRef](#)]
103. Zhu, D.; Zhang, L.; Ruther, R.E.; Hamers, R.J. Photo-illuminated diamond as a solid-state source of solvated electrons in water for nitrogen reduction. *Nat. Mater.* **2013**, *12*, 836–841. [[CrossRef](#)]
104. Huang, X.; Zhao, G.; Wang, G. Sub-nano CoO<sub>x</sub> attached onto WO<sub>3</sub> for efficient photocatalytic and photoelectrochemical water oxidation. *J. Mater. Chem. A* **2017**, *5*, 24631–24635. [[CrossRef](#)]
105. Li, X.; Wang, W.; Jiang, D.; Sun, S.; Zhang, L.; Sun, X. Efficient solar-driven nitrogen fixation over carbon-tungstic-acid hybrids. *Chemistry* **2016**, *22*, 13819–13822. [[CrossRef](#)] [[PubMed](#)]
106. Liang, H.; Zou, H.; Hu, S. Preparation of the W<sub>18</sub>O<sub>49</sub>/g-C<sub>3</sub>N<sub>4</sub> heterojunction catalyst with full-spectrum-driven photocatalytic N<sub>2</sub> photofixation ability from the UV to near infrared region. *New J. Chem.* **2017**, *41*, 8920–8926. [[CrossRef](#)]
107. Shi, A.; Li, H.; Yin, S.; Hou, Z.; Rong, J.; Zhang, J.; Wang, Y. Photocatalytic NH<sub>3</sub> versus H<sub>2</sub> evolution over g-C<sub>3</sub>N<sub>4</sub>/Cs<sub>x</sub>WO<sub>3</sub>·O<sub>2</sub> and methanol tipping the scale. *Appl. Catal. B Environ.* **2018**, *235*, 197–206. [[CrossRef](#)]
108. Zhang, N.; Jalil, A.; Wu, D.; Chen, S.; Liu, Y.; Gao, C.; Ye, W.; Qi, Z.; Ju, H.; Wang, C.; et al. Refining defect states in W<sub>18</sub>O<sub>49</sub> by mo doping: A strategy for tuning N<sub>2</sub> activation towards solar-driven nitrogen fixation. *J. Am. Chem. Soc.* **2018**, *140*, 9434–9443. [[CrossRef](#)] [[PubMed](#)]
109. Li, X.; Yu, J.; Low, J.; Fang, Y.; Xiao, J.; Chen, X. Engineering heterogeneous semiconductors for solar water splitting. *J. Mater. Chem. A* **2015**, *3*, 2485–2534. [[CrossRef](#)]
110. Zhu, W.; Sun, F.; Goei, R.; Zhou, Y. Facile fabrication of RGO-WO<sub>3</sub> composites for effective visible light photocatalytic degradation of sulfamethoxazole. *Appl. Catal. B Environ.* **2017**, *207*, 93–102. [[CrossRef](#)]
111. Gao, C.; Low, J.; Long, R.; Kong, T.; Zhu, J.; Xiong, Y. Heterogeneous single-atom photocatalysts: Fundamentals and applications. *Chem. Rev.* **2020**, *120*, 12175–12216. [[CrossRef](#)] [[PubMed](#)]
112. Fu, J.; Zhu, B.; Jiang, C.; Cheng, B.; You, W.; Yu, J. Hierarchical porous o-doped g-C<sub>3</sub>N<sub>4</sub> with enhanced photocatalytic CO<sub>2</sub> reduction activity. *Small* **2017**, *13*, 1603938–1603947. [[CrossRef](#)] [[PubMed](#)]
113. Tian, B.; Zhen, W.; Gao, H.; Zhang, X.; Li, Z.; Lu, G. Carboxyl-assisted synthesis of Co nanorods with high energy facet on graphene oxide sheets for efficient photocatalytic hydrogen evolution. *Appl. Catal. B Environ.* **2017**, *203*, 789–797. [[CrossRef](#)]

**Disclaimer/Publisher's Note:** The statements, opinions and data contained in all publications are solely those of the individual author(s) and contributor(s) and not of MDPI and/or the editor(s). MDPI and/or the editor(s) disclaim responsibility for any injury to people or property resulting from any ideas, methods, instructions or products referred to in the content.